Journal of
Synchrotron
Radiation

ISSN 1600-5775

Received 4 September 2014
Accepted 14 January 2015

The influence of metallic brazing materials on the strain formation of internally water-cooled X-ray optics

P. Oberta,[a,b]* M. Kittler,[a] V. Áč,[c] J. Hrdý,[a] N. Iragashi,[d] A. C. Scheinost[e] and Y. Uchida[d]

[a]Institute of Physics of the Academy of Sciences of the Czech Republic, Na Slovance 6, CZ-182 21 Praha 8, Czech Republic, [b]Rigaku Innovative Technologies Europe, Novodvorská 994, CZ-142 21 Praha 4, Czech Republic, [c]Department of Physics, Alexander Dubček University of Trenčín, SK-91150 Trenčín, Slovakia, [d]Photon Factory, High Energy Accelerator Research Organization (KEK), 1-1 Oho, Tsukuba, Ibaraki 305-0801, Japan, and [e]The Rossendorf Beamline at ESRF, 38043 Grenoble Cedex 9, France. *E-mail: oberta@fzu.cz

A study of metallic brazing material for internally cooled optics is presented. The study shows the influence of the different material properties on the final quality of the bond in terms of diffracted wavefront distortion, *i.e.* enlargement of the rocking curve. By choosing the proper brazing material and applying the proper brazing conditions, the influence of the brazing material can be fully eliminated. Furthermore the degradation of some brazing material due to the extreme working conditions of the optics is presented. Measurement results from ESRF and KEK confirm the importance of the proper brazing material choice.

Keywords: X-ray optics; high heat load; internal cooling; crystal brazing.

1. Introduction

The increasing flux of new X-ray sources is closely related to higher demands in optics. The most critical effect connected with high-power synchrotron sources is the heat load problem. The high number of absorbed photons creates local temperature gradients which manifest themselves as thermal bumps. The easiest way of minimizing this thermal bump is by developing better cooling schemes. In the past 20 years several cooling schemes have been introduced with various success rates, with cryogenic cooling prevailing (Knapp *et al.*, 1996; Zhang *et al.*, 2013; Chumakov *et al.*, 2014), ahead of water side-cooling (Xu & Wang, 2012) and internal water cooling *via* micro-channels (Bilderback, 1989). Almost all of these cooling schemes went through modifications and upgrades (DiGennaro & Swain, 1990; Oberta *et at.*, 2008*a*); the scientific community introduced also some less used techniques such as pin post cooling (Kuroda *et al.*, 1998) and inclined geometry optics (Hrdý, 1992, Khounsary, 1992; Oberta *et al.*, 2008*b*). The effort presented in the large number of cooling schemes shows that the heat load problem is taken seriously by the optics community. In this paper we will present a study comparing the introduced strain field from the manufacturing process of internally cooled optics.

2. Choice of brazing material

The cooling principle of internally cooled optics is as follows. The optical device (monochromator or mirror) consists of two pieces. The upper part is the diffracting working surface and the lower is the support part. Cooling micro-channels are cut into the bottom of the upper diffraction part and inlet and outlet pipes are brazed to the sides of the lower part. The two counter pieces are brazed together. The most widespread technique of connecting the two pieces is high-temperature brazing. There are also other brazing or bonding techniques available such as glass brazing, Si-on-Si bonding, electrical bonding and explosive bonding (Kim *et al.*, 2004; Schmidt, 1998; Raley *et al.*, 1995; Brida *et al.*, 2005; Xiao *et al.*, 1999; Shu *et al.*, 1995, 2002), but these techniques are not so much used in the synchrotron community. Compared with the semiconductor industry, where most of these methods were developed, for synchrotron use they fail in vacuum compatibility, water leakage or higher complexity in the manufacturing process. In this paper we will present a study of three different metallic brazing materials. The main components of the different brazing materials are aluminium, silver and gold. The choice of a proper brazing material is especially important if the cooled optics is a primary optical device which absorbs most of the source power. In the case of crystal mono-

chromators the introduced heat bump increases the rocking-curve width of the diffracted beam, which leads to a loss of flux and wavefront deformation. Choosing the wrong brazing material may cause additional strain patterns in the diffracted footprint, which further deteriorate the diffracted beam quality. This additional strain pattern matches the structure of the cooling ribs onto the diffracting surface of the optical element as a surface waviness with a period equal to the distance of the cooling ribs. We have investigated three different brazing materials: AlSi(11,7), AgCu(30)Sn(10) and pure Au. Owing to the different material properties, each of the brazing processes was performed under different conditions. In the case of the AlSi(11,7) solder, the fusion temperature at which aluminium creates a eutectic material with silicon is $T = 577^{\circ}$C, hence we used a brazing temperature of $T = 700^{\circ}$C with a 38 µm-thick foil. Prior to the brazing process the brazing surfaces were deposited with a 10 µm layer of pure aluminium. The number (11,7) stands for the percentage ratio of the melted silicon in aluminium. In the case of the AgCu(30)Sn(10) solder material we used a 60 µm-thick foil with a fusion point between $T = 612^{\circ}$C and 780°C. Prior to the brazing process the brazing surfaces were deposited with a 10 µm layer of pure silver. The brazing temperature here was $T = 750^{\circ}$C, so we did not reach the temperature of the eutectic alloy, with consequences discussed later. Other candidates including a silver component were, for example, AgCu(33)Sn(25) with a fusion point of $T = 580^{\circ}$C (not available as foil) or AgCu(28)Ge(2)Co(0.3) with a fusion point of $T = 780^{\circ}$C. In the case of the Au solder material we used a 20 µm-thick foil, with a fusion point of $T = 370^{\circ}$C. Prior to the brazing process we deposited a 0.5 µm layer of Au on the brazing surface. The brazing process took place under a temperature of $T = 550^{\circ}$C for a period of 45 min. The increase of the temperature from 0°C to 550°C took place over a period of 2.5 h. All three samples had a cube shape with a groove structure of 0.8 mm channel width and 1.6 mm rib thickness. The channel height was 2.0 mm with a 2.0 mm-thick silicon layer above the micro-channels. The sample was made of Si(111) material (Fig. 1).

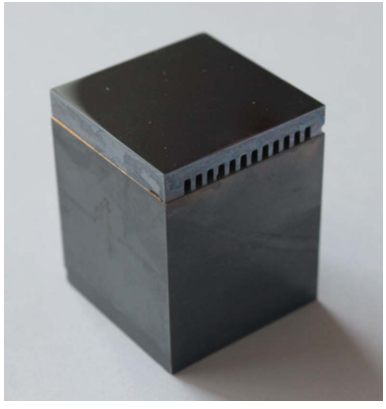

Figure 1
Cross section of a monochromator crystal with micro-channel cooling geometry. The diffracting Si(111) crystal is brazed to the support Si block with a metallic brazing material, in this case 20 µm of gold.

Table 1
Rocking-curve broadening (arcsec) compared with the theoretical value for Cu $K\alpha$ radiation [Si(111) = 7.395 arcsec, Si(333) = 1.989 arcsec (Caciuffo *et al.*, 1987)] of three different metallic brazing materials for the crystallographic orientations Si(111) and Si(333) for two different Si layer thicknesses above the cooling micro-channels (1 mm and 2 mm).

	Solder material		
	Ag	Al	Au
2 mm above cooling channels			
(111)	1.19	0.80	0.39
(333)	0.48	0.46	0.18
1 mm above cooling channels			
(111)	2.20	1.64	0.51
(333)	0.57	0.85	0.11

Because the aim of the brazing process is to create a eutectic connection between the brazing materials, in our case the metallic foil and the silicon, the connection undergoes extreme heat changes. Owing to the different material properties of the various materials a strain pattern can be created during the cooling process. We have performed two measurements to quantify the strain amount. The first one is the rocking curve width measurement, where we compare the broadening of the rocking curve with the theoretical rocking curve, and the second measurement is X-ray topographical diffraction images. As the X-ray source we used a laboratory Seifert Cu X-ray tube (8 keV, Cu $K\alpha_{1,2}$), with a double-crystal arrangement and a Rigaku XSight Micron detector. The first crystal of the double-crystal arrangement was a flat Si(111) crystal and the second crystal was a brazed monochromator sample. The top surface of our test sample is a Si(111) crystal. The two crystals were in a non-dispersive arrangement. The micro-channels were parallel to the X-ray beam because of the higher cooling efficiency as compared with the micro-channels perpendicular to the source (Hrdý & Plešek, 1998; Micha *et al.*, 2013). Table 1 shows the measured enlargement of the full width at half-maximum of three different braze materials for Si(111) and Si(333) crystallographic plane orientations.

As can be seen, the largest rocking-curve broadening due to the strain introduced by the brazing process was in the case of the silver brazing material, more than 1 arcsec (5.7 µrad). In the case of the aluminium brazing material the broadening was 0.8 arcsec (3.8 µrad). The best results were obtained with the gold brazing material, only 0.39" (1.8 µrad). One of the reasons why the gold brazing material has the lowest strain map (none is visible, but the rocking-curve enlargement indicates its presence) is that gold has the lowest fusion point. So the thermal stress introduced to the two different materials is low compared with the other metallic materials. Fig. 2 shows the topographic images of the diffracted surface from the Si(111) planes. The topographic pictures are in gradient colours to emphasize the inhomogeneous reflectivity distribution, due to the present strain. In the case of the aluminium brazing, the reflectivity is relatively uniform, but one can see the structure of the cooling micro-channels. This means that at the edges of the cooling channels exists a local strain field. In the case of the silver brazing material the reflectivity distri-

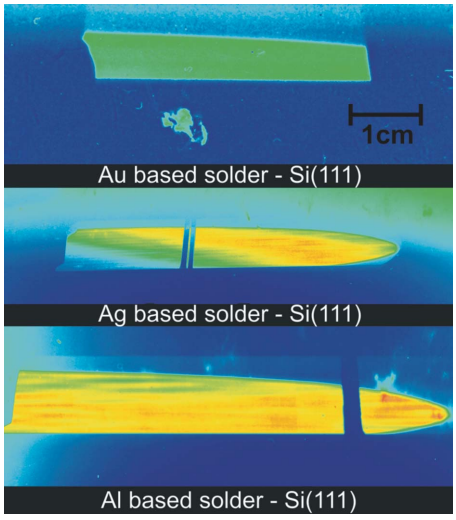

Figure 2
Topographical images of the Si(111) diffraction from an internally cooled sample brazed with gold (top), silver (middle) and aluminium material (bottom).

bution is very non-uniform, with a visible micro-channels structure. On the other hand the reflectivity distribution of the gold brazed samples is very smooth and uniform with no visible micro-channel structure beneath the silicon surface.

From the point of view of the rocking-curve broadening and the diffraction topographic images the most promising candidate for a stress-free brazing connection of two silicon pieces is a gold bond. During the operation time at synchrotron and laboratory sources further effects occur connected to the choice of brazing material. An internally cooled optics is employed in a highly ionized environment. Therefore the choice of a proper brazing material is not only critical from the mechanical point of view (strain creation) but also from the point of view of chemical stability. The radiation passing through the optical device interacts with the cooling medium (de-ionized water) and can lead to the creation of chemical radicals. These radicals can interact with the brazing material which can lead to corrosion of the inlet and outlet pipes and possible crystal growth inside the micro-channels. Most probably this was the case in the internally cooled monochromator at the ROBL beamline at the ESRF, which had an aluminium-based brazing material. After an X-ray fluorescence analysis of the debris we found out that the main component was aluminium. The combination of the internal crystal growth and the debris in the cooling medium started to plug the cooling micro-channels, which caused the formation of internal pressure and ultimately to a deformation of the diffracting surface or even cracking of the crystal surface. Depending on the degree of the deformation, the Bragg diffraction condition can be violated in certain areas of the crystals surface. This can lead to reflectivity variation, which was also observed at the bending-magnet beamline ROBL at ESRF (Fig. 3). The topographic image in Fig. 3 (top left) was collected at 25 keV with a slit opening of 3 mm × 20 mm, with the storage ring operating at 160 mA in multibunch mode. We

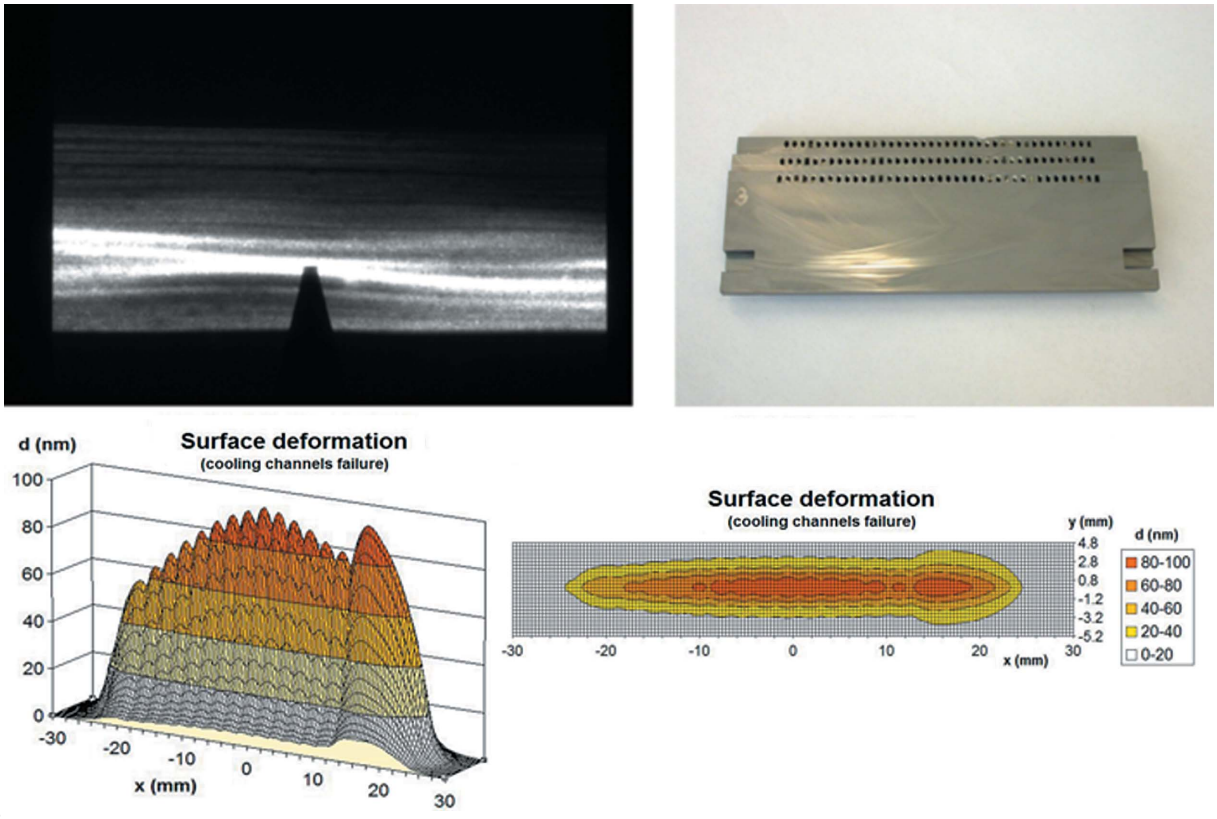

Figure 3
Finite-element analysis simulation of the surface deformation distribution in the case when several cooling micro-channels are plugged due to debris. The subsequent strain creation can lead to a non-homogeneous reflectivity distribution.

have simulated these conditions and created a finite-element analysis simulation of the surface deformation of the monochromator. The simulations were performed in such a way that they copy the real situation of the transversely cut monochromator (Fig. 3, top right), where the flow rate of the partially plugged cooling micro-channels decreased to 0%, 40%, 10% and 40%. Because we have no detailed information about all the cooling micro-channels, a realistic simulation of the surface deformation is very difficult. However, even this partial plugging of four cooling micro-channels induced a surface distortion with peak deformation reaching up to 100 nm (Fig. 3, bottom).

As has already been mentioned above, in the case of the silver-based brazing material, the fusion temperature is between $T = 612^{\circ}$C and 780°C. The employed high-temperature oven could reach a maximum temperature of $T = 800^{\circ}$C, but due to safety reasons only a temperature of $T = 750^{\circ}$C was reached. The resulting brazing appeared to be stable, and no release after mechanical manipulation was observed. We performed the rocking-curve measurement and recorded the topographical images using the silver-based sample. After ageing this sample on the shelf for several months, we observed that the two brazed silicon pieces released from the brazing foil. The most probable explanation is that not having reached the fusion point led to a relaxation of the bond.

At the BL-5A beamline for high-throughput macromolecular crystallography at the KEK Photon Factory synchrotron source in Japan we measured two internally cooled monochromators with two different brazing materials. The geometry of the internal cooling structure was different. The cooling micro-channels of the aluminium brazed monochromator had a width of 0.25 mm and a rib width of 0.2 mm. The micro-channels of the gold brazed monochromator had a width of 0.13 mm and a rib width of 0.17 mm. The aluminium brazed monochromator had a thickness above the cooling channels of 2.0 mm and the gold brazed monochromator had a thickness of 1.0 mm (Fig. 4). The used X-ray source was a multipole wiggler, with a 120 mm period (21 periods), 14.4 T field and a maximal flux of 6.6×10^{11} photons s^{-1} at 450 mA (slits aperture 0.2 mm × 0.2 mm). The cooling water flow was 2.8 L min^{-1}. We performed two measurements at an energy of $E = 12.6$ keV ($\Theta = 9^{\circ}$ incident Bragg angle). The estimated total power at 450 mA was 152 W and 8 W at a gap opening of 26.4 mm and 70 mm, respectively. There was also a difference

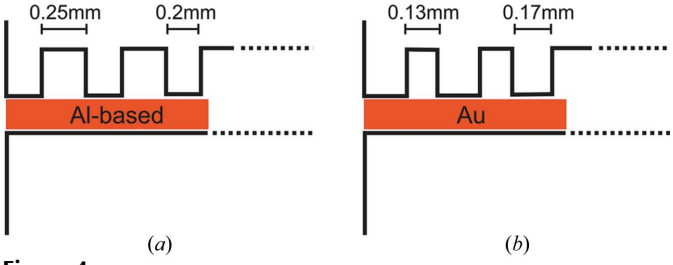

Figure 4
Schematic drawing of the water-cooled monochromator design used. Dimensions of (*a*) the aluminium-based solder monochromator and (*b*) the gold brazed monochromator.

Table 2
Rocking-curve widths (arcsec) of the aluminium-based brazed monochromator and of the gold brazed monochromator at wiggler gap openings of 26.4 mm and 70 mm; the enlargement of the rocking curve compared with the theoretical rocking-curve width of a Si(111) diffraction is due to heat load and brazing strain.

Wiggler gap (mm)	Al based (arcsec)	Au based (arcsec)	Theory (FWHM arcsec)	Δ_{Al} (arcsec)	Δ_{Au} (arcsec)
26.4	10.1	7.2	6.1	4	1.1
70.0	7.4	6.5		1.3	0.4

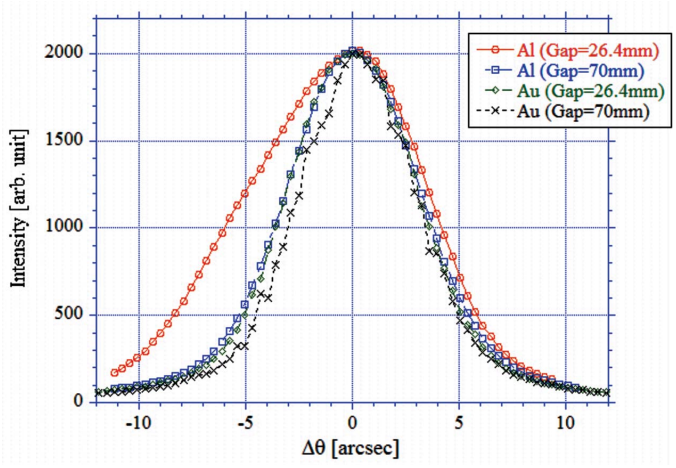

Figure 5
Full width at half-maximum of the rocking-curve measurement of an aluminium and a gold brazed monochromator at an energy of 12.6 keV. The measurements were performed at wiggler gaps of 26.4 mm (red and green plot) and 70 mm (blue and black plot). The intensity is normalized to the 26.4 mm gap-opening aluminium intensity.

in the current during the measurement of the aluminium brazed monochromator ($I = 350$ mA) and the gold brazed monochromator ($I = 450$ mA). Fig. 5 shows the rocking-curve measurement of the aluminium brazed monochromator, with FWHMs of 10.1 arcsec (26.4 mm) and 7.4 arcsec (70 mm). The FWHMs of the gold brazed monochromator were 7.2 arcsec (26.4 mm) and 6.5 arcsec (70 mm). The theoretical FWHM for energy $E = 12.6$ keV is 6.1 arcsec. An overview of the measurements is shown in Table 2.

3. Surface preparation effects

Another approach of how to lower potential strain creation due to internally cooled optics manufacturing is to prepare a proper brazing surface. Let us call the following surface preparation process the standard process (method A). After cutting the proper crystal shape, the surface is mechano-chemically ground. To minimalize the sub-surface strain one etches the surface and the last step is surface polishing to optical surface quality. This approach has the drawback that the two crystal surfaces which are made for common brazing have a different surface structure. Each optical surface has a specific surface roughness in three spatial frequency domains which can be viewed in the PSD function. In the mid- and

Table 3
Rocking-curve broadening.

The laboratory source was a Cu $K\alpha_1$ X-ray tube (8.05 keV). The crystal orientations were Si(111) and Si(333). We investigated both geometries with cooling micro-channels oriented parallel to the source and perpendicular to the source.

Si orientation	Method A (arcsec)	Method B (arcsec)	
(111)	0.69	0.39	Micro-channels parallel
(333)	0.37	0.18	
(111)	1.50	0.80	Micro-channels perpendicular
(333)	0.93	0.21	

high-frequency domain the waviness can have opposite amplitude for the two crystal pieces. This can lead to specific points in the brazing connection where more brazing material is necessary. With this approach we prepared one sample. Another sample was prepared using a different approach (method B). We replaced the mechano-chemical grading process by grinding the counter parts against each other in the direction of the cooling micro-channels, thereby creating guide grooves. In this way the two counter parts which are made for brazing fit better together (Fig. 6). We prepared two identical samples (Fig. 1) with a gold brazing layer of 20 µm. The diffracting surface was the Si(111) crystallographic plane. One sample was prepared using method A and the other using method B.

We measured the rocking curve of the Si(111) and the Si(333) crystal orientations using a Cu $K\alpha$ source. The orientation of the cooling micro-channels also has an impact on the rocking-curve enlargement, so both orientations were investigated: one with the cooling micro-channels oriented parallel to the source and the other with them oriented perpendicular to the source. Table 3 shows the rocking-curve broadening of the measured rocking curve from the theoretical FWHM in arcsec. One can see that the surface preparation method B gives better quantitative results in all four cases.

Fig. 7 shows microscope images of the vertical cut through the sample. We can see the detail of the metallic bond prepared using the two methods. The upper two images are cross sections from method A and the lower two images are cross sections from preparation method B. In case of method B the metallic bond shows fewer imperfections. Method A creates a flatter surface compared with a 'toothy' surface by

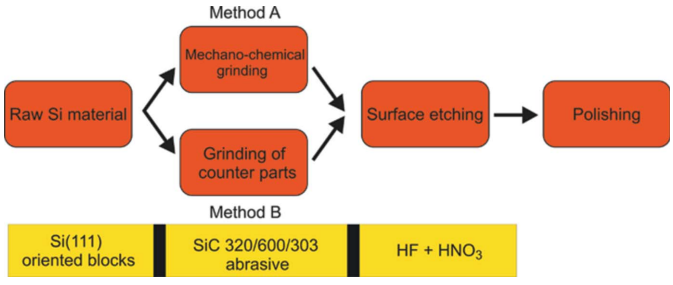

Figure 6
Schematic approach and difference in the surface preparation methods A and B.

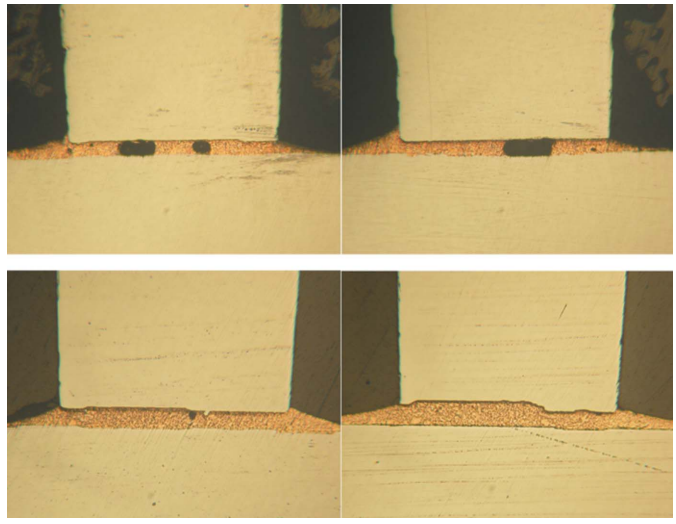

Figure 7
Microscopic images of the gold bond connection showing the difference in the brazing connection between the surface preparation methods A (upper two) and B (lower two).

method B. The air pockets visible from method A are due to capillary forces which tear apart the thin metallic layer. In the case of an uneven surface these capillary forces are reduced. Because the brazed connection acts with a vertical force on the crystal surface, each air pocket (brazing imperfection) represents a deviation in the strain field of the brazed connection and has a direct influence on the FWHM of the diffraction curve.

4. Conclusion

We have investigated three metallic materials and their influence on the strain creation of internally cooled optics. The manufacturing process of the internally cooled optics was high-temperature brazing. From the three investigated brazing materials based on aluminium, silver and gold, the most promising is gold, for which the strain due to manufacturing is almost fully eliminated. Also presented and explained are effects which occur during the operation of such manufactured optics at synchrotron facilities (ESRF and KEK). The impact of the surface preparation method is also discussed. Two surface finishing methods are compared. The amount of broadening of the measured rocking-curve FWHM shows that the grinding process has a lower influence on the performance of the internally cooled optics when the two counter pieces are ground against each other and create a non-flat structure on the crystal surface.

We would like to thank Blahomil Lukáš from the ABB Company in Prague for providing the silicon crystals and for partial sample preparation. We would also like to thank the optical workshop of the Institute of Physics of the Academy of Sciences of the Czech Republic for the sample preparation.

References

Bilderback, D. H. (1989). *Rev. Sci. Instrum.* **60**, 1977.

Brida, S., Metivet, S., Petit, D. & Stojanovic, O. (2005). *Microsyst Technol.* **12**, 59–62.
Caciuffo, R., Melone, S., Rustichelli, F. & Boeuf, A. (1987). *Phys. Rep.* **152**, 1–71.
Chumakov, A. I., Sergeev, I., Celse, J.-P., Rüffer, R., Lesourd, M., Zhang, L. & Sánchez del Río, M. (2014). *J. Synchrotron Rad.* **21**, 315–324.
DiGennaro, R. & Swain, Th. (1990). *Nucl. Instrum. Methods Phys. Res. A*, **291**, 305–312.
Hrdý, J. (1992). *Rev. Sci. Instrum.* **63**, 459–460.
Hrdý, J. & Plešek, J. (1998). *J. Synchrotron Rad.* **5**, 667–669.
Khounsary, A. M. (1992). *Rev. Sci. Instrum.* **63**, 461–464.
Kim, H. S., Blick, R. H., Kim, D. M. & Eom, C. B. (2004). *Appl. Phys. Lett.* **85**, 2370–2372.
Knapp, G. S., Jennings, G. & Beno, M. A. (1996). *Rev. Sci. Instrum.* **67**, 3352–3354.
Kuroda, M., Yamazaki, H., Suzuki, M., Kimura, H., Kagaya, I., Yamashita, C. & Ishikawa, T. (1998). *J. Synchrotron Rad.* **5**, 1211–1214.
Micha, J.-S., Geaymond, O. & Rieutord, F. (2013). *Nucl. Instrum. Methods Phys. Res. A*, **710**, 155–160.
Oberta, P., Áč, V. & Hrdý, J. (2008*b*). *J. Synchrotron Rad.* **15**, 8–11.
Oberta, P., Áč, V., Hrdý, J. & Lukáš, B. (2008*a*). *J. Synchrotron Rad.* **15**, 543–548.
Raley, N. F., Davidson, J. C. & Balch, J. W. (1995). *Proc. SPIE*, **2639**, 40–45.
Schmidt, M. A. (1998). *Proc. IEEE*, **86**, 1575–1585.
Shu, D., Li, Y., Ryding, D., Kuzay, T. M. & Brasher, D. (1995). *Rev. Sci. Instrum.* **66**, 1783–1785.
Shu, D., Ramanathan, M. & Haeffner, D. R. (2002). *Rev. Sci. Instrum.* **73**, 1584–1586.
Xiao, Z.-X., Wu, G.-Y., Li, Z.-H., Zhang, G.-B., Hao, Y.-L. & Wang, Y.-Y. (1999). *Sens. Actuators A*, **72**, 46–48.
Xu, Z. & Wang, N. (2012). *J. Synchrotron Rad.* **19**, 428–430.
Zhang, L., Sánchez del Río, M., Monaco, G., Detlefs, C., Roth, T., Chumakov, A. I. & Glatzel, P. (2013). *J. Synchrotron Rad.* **20**, 567–580.